MEASUREMENT OF MACRO-SCALE INDENTATION MODULUS USING THE PRIMARY HARDNESS STANDARD MACHINES AT INRIM

IMEKO 23rd TC3, 13th TC5 and 4th TC22 International Conference
30 May to 1 June, 2017, Helsinki, Finland

MEASUREMENT OF MACRO-SCALE INDENTATION MODULUS USING THE PRIMARY HARDNESS STANDARD MACHINES AT INRIM

Alessandro Schiavi[1], *Claudio Origlia*[1], *Alessandro Germak*[1],
Giulio Barbato[2], *Giovanni Maizza*[3],*Gianfranco Genta*[2], *Roberto Cagliero*[4], *Gianluca Coppola*[1,2]

[1]INRIM – National Institute of Metrological Research, STALT, Italy, a.schiavi@inrim.it
[2]Politecnico di Torino DIGEP, Italy
[3]Politecnico di Torino, DISAT, Italy
[4]INSTM, Italy

Abstract: In this paper it is described the experimental procedure and the statistical method for the measurement of indentation modulus by using the primary hardness standard machine at INRIM, in the macro-scale range. Indentation modulus is calculated on the basis of Doerner-Nix linear model and from accurate measurements of indentation load, displacement, contact stiffness and Vickers hardness impression imaging. Load is provided by dead-weight masses and displacement is measured by a laser-interferometric system, perpendicular with respect to the Vickers pyramid vertex. The geometrical dimension of the Diamond Pyramid Hardness (DPH) impression is measured by means of a micro-mechanical system and optical microscopy imaging technique. Applied force and indentation depth are measured simultaneously, 16 Hz of sampling rate, and the resulting indentation curve is obtained. Preliminary tests are performed on metals and alloys samples. Considerations and comments on the accuracy of the proposed method and analysis are discussed.

Keywords: Hardness, indentation modulus, macro-scale.

1. INTRODUCTION

Elastic properties of materials, in mechanical engineering and material science, can be evaluated by means of several different experimental techniques, based on static, quasi-static and dynamic methods. These techniques involve, as an example, measurements of tensile or compressive stress-strain, resonance methods and NDT-based methods, such as measurements of acoustic waves propagation speed in solids or phonon detection. Moreover also techniques involving instrumented indentation (from nano- to macro- scale) are used to evaluate elastic properties of materials and procedures are collected in ISO 14577-1 [1] (for metallic materials). As it is known, elastic response of materials may vary as a function of different experimental technique used, measurement procedures and other boundary conditions, as a consequence, relevant differences in Young's modulus values can be easily achieved. In the case of instrumented indentation, ISO selected the specific name of "Indentation modulus" and the symbol E_{IT} for underlining possible differences. From the metrological point of view, "hardness" is actually the only measurement collected in the international comparison of CMC (Calibration and Measurement Capabilities) of the BIPM. The possibility to evaluate the elastic properties from consolidate and accurate experimental procedures is a promising attempt, in order to reduce some sources of uncertainty and dispersion of experimental results.

Observation of elastic recovery effects in indentation test, date back 1961, by Stilwell and Tabor [2]. First attempts to measure hardness and elastic modulus by instrumented indentation can be traced back in 1983: Pethicai, Hutchings and Oliver, investigating a method to evaluate hardness at nano-scale level, showed that depth-sensing indentation allows to build load-displacement curve, strongly related to the typical stress-strain diagrams of materials [3]. In 1986, Doerner and Nix, improved the methods by using a high resolution depth-sensing instrument [4] and in 1992 Oliver and Pharr introduced a practical model for measuring hardness and elastic modulus, by instrumented indentation [5]. At present day these models are included in the ISO 14577, nevertheless several important changes have been proposed during the last decades, improving both the accuracy and the application field of the models [6-9].

In this paper elastic properties of copper alloy, aluminum alloy, brass and stainless steel samples, in terms of indentation modulus, are investigated from macro-indentation test. Measurements are performed using the primary hardness machine, designed and realized at INRIM.

2. INDENTATION MODULUS

Indentation modulus, E_{IT}, is properly the elastic response of a material when subjected to the action of a concentrated load in a single point. Occurring deformations are not linear, as a consequence indentation modulus represents a reasonably close estimation of Young's modulus.

In the following, as shown in equation (1), indentation modulus is determined, in macro-scale range, from Vickers hardness test only, by using a square based diamond pyramid indenter, having a measured vertex angle α=135.9°,

between opposite faces. The diamond Young's modulus is assumed to be E_i=1140 GPa and Poisson ratio ν_i=0.07. Summarizing, indentation modulus is defined as:

$$E_{IT} = \frac{a}{(b \cdot c \cdot d) - e} \quad (1)$$

where, explicating all parameters on the basis of known constant, it follows that:

$$a = 1 - \nu_s^2 \quad (2)$$

$$b = 4 \cdot \tan(\alpha / 2) \quad (3)$$

$$c = \left(S \cdot \sqrt{\pi}\right)^{-1} \quad (4)$$

$$d = \left[h_{\mathrm{MAX}} - (C_f \cdot F_{\mathrm{MAX}}) - \varepsilon \frac{F_{\mathrm{MAX}}}{S} \right] \quad (5)$$

$$e = \frac{1 - \nu_i^2}{E_i} \quad (6)$$

As it is possible to notice, indentation modulus depends on several experimental values from measurements, and empirical values, calculated from indentation curve best-fit:

- Parameter *a* depends on the Poisson ratio ν_s, of tested material. It is possible to refer, with the due caution, to data available in technical literature, for a rough estimation.
- Parameter *b* is a constant and depends on the actual angle between opposite faces of the Vickers indenter.
- Parameter *c* depends on the contact stiffness *S*. This quantity is the incremental ratio between unloading force and related displacement at maximum depth of indentation h_{MAX}, i.e. $S=\partial F/\partial h|_{h\mathrm{MAX}}$, and it is calculated from the best-fit of the unloading indentation curve.
- Parameter *d* depends on the empirical value of contact stiffness *S* and on the experimental values of maximum applied force, F_{MAX}, maximum depth of indentation, h_{MAX}, and on the elastic deformation occurring in the testing machine, C_f, also called frame compliance; coefficient ε=0.75 depends on the geometry of the indenter.
- Parameter *e* depends on the Young's modulus and on the Poisson ratio of the Vickers indenter.

Several methods are proposed in order to evaluate the frame compliance C_f, both in Standard [1] and in literature [10]. In Section 3 it is shown in detail the method used in this paper to accurately calculate the frame compliance, on the basis of experimental data of Vickers impression shape.

In Figure 1 and Figure 2 the experimental data needed for the model implementation are depicted. In Figure 1 a typical Vickers hardness impression and in Figure 2 an experimental indentation curve, as a function of force and displacement, are shown.

Figure 1: Microscopic image of a typical Diamond Pyramid Hardness (DPH) impression from a Vickers hardness test on a metallic surface.

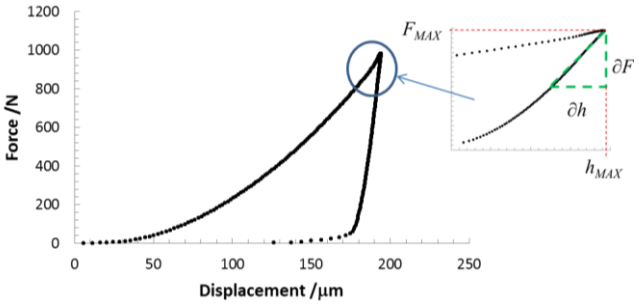

Figure 2: Typical force-displacement indentation curve with the indication of the quantities used in the model.

Once the maximum applied force F_{MAX}, and the maximum depth of indentation h_{MAX} are known, indentation modulus, E_{IT}, can be calculated from experimental data of Vickers impression geometrical dimensions (Figure 1, in general the two diagonals), and from the slope of the indentation curve (Figure 2, during the unloading path). In particular an accurate evaluation of contact stiffness *S* depends on the best-fit of the unloading path. ISO 14577-1 recommends two methods to fit the curve, by a linear model (Doerner-Nix method), taking into account the initial 20% of the unloading curve, and by a power-law model (Oliver-Pharr method), taking into account a range between 50% and 80% of the unloading curve. The linear model does not determine the slope at h_{MAX}, but estimate the slope at the centre of the data interval, but, with the reduction from 30% to 20% of the last standard release it is a good approximation of the ideal value. The power-law model is relied to the depth of the unloading point, which has an high uncertainty both for its measurement and for the last part of

elastic recovery, therefore in this paper only the linear model is used in order to fit the unloading curve.

3. COMPLIANCE

Frame compliance C_f is an experimental quantity taking into account the whole deformation occurring in the testing machine during the indentation test. In order to estimate the actual frame compliance in this paper two methods are compared, the first according to Standard ISO 14577-1, based on a series of loading and unloading cycles, the latter according to literature [11], based on the indentation depth of the Vickers impression.

In general terms, frame compliance C_f can be considered as the difference between the total compliance C_{tot} and the sample compliance C_s [12], as follows

$$C_f = C_{tot} - C_s = \left.\frac{dh}{dF}\right|_{F=F_{MAX}} - \frac{\sqrt{A_p}}{S}\frac{\sqrt{H_{IT}}}{F_{MAX}} \qquad (7)$$

In which total compliance C_{tot} is determined as the reciprocal of contact stiffness, measured after a series of loading and unloading cycles on a single point, and the sample compliance C_s depends on the standard indentation hardness H_{IT}, on the contact stiffness S and on the contact area A_p of the Vickers indenter, which is calculated as:

$$A_p = 4.95\left(h_{MAX} - 0.75\frac{F_{MAX}}{S}\right) \qquad (8)$$

On the basis of experimental data, as it is shown in the Section 5, the compliance of the sample C_s is negligible with respect to total compliance C_{tot}, therefore it can be assumed that $C_f \approx dh/dF$.

By measuring the slope of indentation curve, after several repetitions, frame compliance is determined on the basis of a linear regression, as shown in Figure 3.

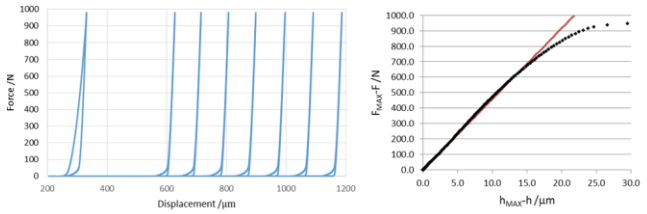

Figure 3: Series of loading-unloading cycles on a single point and linear regression of the last reversed unloading curve.

The frame compliance is calculated after several cycles of loading and unloading, according to Standard, on a stainless steel sample. The reciprocal of contact stiffness, as shown in relation (7), allows to calculate the value of frame compliance. In this study $C_f = 22.1 \cdot 10^{-9}$ m/N. Taking into account that (see Section 6) experimental values of sample compliance C_s range between 10^{-13} m/N and 10^{-12} m/N, it is possible to assume that $C_f \approx C_{tot}$, as previously suggested.

Frame compliance C_f is also calculated on the basis of measured indentation depth. An automatic micro-mechanical system and an optical microscopy system imaging technique is used for Vickers impression detection. Diagonals lengths are measured with an accuracy of 0.1 µm. In Figure 4 the optical system and the image processing are shown.

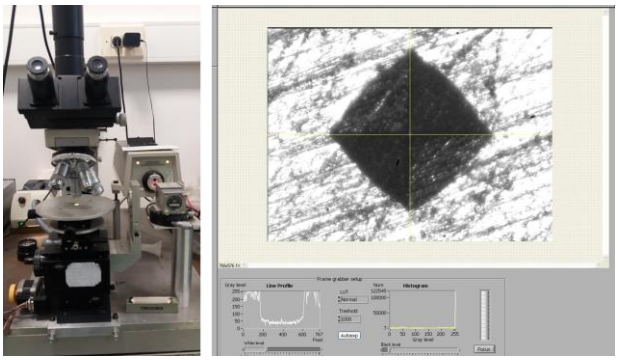

Figure 4: Optical microscopy system and imaging technique for measuring geometrical dimension of the impressions.

Assuming that, for many metallic materials, the elastic recovery upon unloading induces very small elastic deformation at the corners of a Vickers indentation, therefore, between the loaded and unloaded condition, a negligible change in the diagonal dimensions is expected [13]. As a consequence frame compliance C_f can be estimated from the following equation:

$$C_f = \frac{h_{MAX} - h_v}{F_{MAX}} \qquad (9)$$

where h_v is the indentation depth measured from the actual Vickers hardness impression. In particular, by measuring the length of the sides impression l, indentation depth h_v is given by:

$$h_v = \frac{l}{2} \cdot \cot(\alpha/2) \qquad (10)$$

Side impression length l is generally calculated from the two measured diagonal d, since a greater accuracy can be achieved:

$$l = \frac{d_1 + d_2}{2}\sin\frac{\pi}{4} \qquad (11)$$

where d_1 and d_2 are the two measured diagonal of the Vickers impression and d_{av} is the average diagonal.

Data of frame compliance C_f calculated on the basis of relation (9) from the shape of the Vickers impression, range from ~10^{-10} m/N up to ~10^{-7} m/N, as shown in Table II-V.

Data in bracket (referred to HV3) are considered outliers, further analysis are under investigation. In the graph of Figure 5, a comparison between standard method and the proposed method is shown.

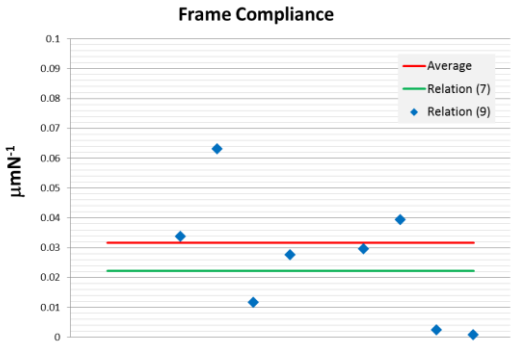

Figure 5: Comparison between frame compliance calculated from relation (7) and relation (9). The red line is the average value of compliance measured from relation (9).

The difference is probably due to the fact that relation (9) determine the slope from the F_{MAX} and F=0 points, therefore is affected by the elastic recovery of the last part of unloading phase.

4. PRIMARY HARDENESS STANDARD MACHINE

Measurements of indentation modulus are performed by using the INRIM Primary Hardness Standard machine. The activities regarding the realization and the improvement of the Standard machine at INRIM, date back to early 1970s and continued until the present day. Technical features and metrological characterization in detail are summarized in [14-16]. In Figure 6 the whole system and some details are shown.

Figure 6: INRIM Primary Hardness Standard machine, the anvil and a Vickers indenter.

The system generates forces by moving a series of dead weight masses and a laser interferometric system is used for indentation depth measurements.

Force measurement are monitored by a load cell and experimental values are determined with an accuracy within 0.01%. The laser beam is aligned on the measurement axis and experimental values are determined with a resolution of 0.02 μm.

Force and indentation depth are monitored in real time and date are recorded with a sampling rate of 16 Hz.

In this context, Vickers hardness measurements with 100 kg, 30 kg and 3 kg mass (i.e. 980.6 N, 294.2 N and 29.4 N), are performed in order to define the indentation modulus. Deformations, in terms of compliance, of the whole system is about 0.03 μm with a load of 1 kN.

5. MATERIALS

Materials tested in this work are copper alloy, aluminium alloy, stainless steel and brass. Young's modulus E and Poisson ratio ν_s of tested materials were previously determined on the basis of accurate measurements of longitudinal c_l and transversal c_t sound speed waves in solids [17], at room conditions. Although some systematic differences between dynamic and static moduli can be achieved, reference data can be considered accurate enough and useful for the proposed comparison method, since overall uncertainties are lower than 1%. In Table I reference data of tested alloys are shown.

Table I: Reference data of tested alloys.

	Stainless steel	Aluminum Alloy	Copper alloy	Brass
ρ /kgm^{-3}	7914.1	2806.4	8932.5	8296.1
c_l /ms^{-1}	5759.1	6294.7	4779.0	4520.3
c_t /ms^{-1}	3146.2	3082.4	2247.8	1842.1
E /GPa	201.7	71.6	122.6	78.9
ν_s /–	0.287	0.342	0.358	0.400

The dynamic Poisson ratio ν_s is calculated from the relation:

$$\nu_s = \frac{1 - 2\left(\frac{c_l}{c_t}\right)^2}{2 - 2\left(\frac{c_l}{c_t}\right)^2} \qquad (12)$$

values of Poisson ratio ν_s, listed above, have been used in relation (2), for the indentation modulus calculation.

Dynamic Young's modulus E is calculated from the following relation:

$$E = 2\rho c_l^2 (1 + \nu_s) \qquad (11)$$

6. EXPERIMENTAL RESULTS

Measurements of indentation modulus are performed at 980.6 N, 294.2 N and 29.4 (which correspond to the maximum applied force, F_{MAX}) and occurring maximum indentation depth h_{MAX} is measured both by a laser interferometric system and from the hardness impression, h_v. Moreover the average diagonal d_{av} and the calculated square side l are shown. Values of frame compliance C_f, from relation (9), contact area A_p, sample compliance C_s and hardness H_{IT}, are also shown. Value of contact stiffness $S=\partial F/\partial h$ (evaluated at h_{MAX}), is calculated on the basis of linear model. In the following Tables are collected all the experimental and empirical data of 4 metallic samples, used in relation (1) for model implementation.

Table II: Data of Stainless steel 304

	(HV3)	(HV30)	(HV100)
F_{MAX} /N	29.4	294.2	980.6
h_{MAX} /μm	43.5	112.1	181.0
h_v/μm	23.2	80.1	147.8
d_{av}/μm	162.3	559.6	1032.3
l /μm	114.8	395.7	729.9
A_p /m	$4.38\cdot10^{-8}$	$2.83\cdot10^{-7}$	$7.19\cdot10^{-7}$
C_s /mN^{-1}	$5.74\cdot10^{-12}$	$5.08\cdot10^{-13}$	$1.51\cdot10^{-13}$
H_{IT}	210.8	177.5	173.9
C_f /mN^{-1}	$(6.89\cdot10^{-7})$	$1.09\cdot10^{-7}$	$3.38\cdot10^{-8}$
S /Nm^{-1}	$1.80\cdot10^{7}$	$4.75\cdot10^{7}$	$7.56\cdot10^{7}$

Table III: Data of Copper alloy

	(HV3)	(HV30)	(HV100)
F_{MAX} /N	29.4	294.2	980.6
h_{MAX} /μm	43.6	155.3	320.4
h_v/μm	41.7	151.9	293.3
d_{av}/μm	291.4	1060.5	2047.9
l /μm	206.0	749.8	1448.1
A_p /m	$4.44\cdot10^{-8}$	$5.64\cdot10^{-7}$	$2.39\cdot10^{-6}$
C_s /mN^{-1}	$2.69\cdot10^{-12}$	$2.92\cdot10^{-13}$	$1.15\cdot10^{-13}$
H_{IT}	65.4	49.4	44.2
C_f /mN^{-1}	$(6.31\cdot10^{-8})$	$1.16\cdot10^{-8}$	$2.77\cdot10^{-8}$
S /Nm^{-1}	$2.15\cdot10^{7}$	$6.15\cdot10^{7}$	$9.14\cdot10^{7}$

Table IV: Data of Aluminum alloy

	(HV3)	(HV30)	(HV100)
F_{MAX} /N	29.4	294.2	980.6
h_{MAX} /μm	32.0	89.6	187.7
h_v/μm	25.4	80.9	149.1
d_{av}/μm	177.4	565.1	1041.4
l /μm	125.4	399.6	736.4
A_p /m	$2.16\cdot10^{-8}$	$1.64\cdot10^{-7}$	$7.27\cdot10^{-7}$
C_s /mN^{-1}	$7.12\cdot10^{-12}$	$6.36\cdot10^{-13}$	$2.39\cdot10^{-13}$
H_{IT}	176.6	174.1	170.9
C_f /mN^{-1}	$(2.26\cdot10^{-7})$	$2.95\cdot10^{-8}$	$3.94\cdot10^{-8}$
S /Nm^{-1}	$9.32\cdot10^{6}$	$2.86\cdot10^{7}$	$4.75\cdot10^{7}$

Table V: Data of Brass

	(HV3)	(HV30)	(HV100)
F_{MAX} /N	29.4	294.2	980.6
h_{MAX} /μm	25.9	103.7	188.5
h_v/μm	32.5	103.0	187.8
d_{av}/μm	227.1	719.2	1311.6
l /μm	160.6	508.5	927.4
A_p /m	$1.47\cdot10^{-8}$	$2.39\cdot10^{-7}$	$7.79\cdot10^{-7}$
C_s /mN^{-1}	$2.63\cdot10^{-12}$	$3.79\cdot10^{-13}$	$1.30\cdot10^{-13}$
H_{IT}	106.3	106.0	107.7
C_f /mN^{-1}	$(-2.26E^{-07})$	$2.49\cdot10^{-9}$	$6.92\cdot10^{-10}$
S /Nm^{-1}	$1.62\cdot10^{7}$	$4.51\cdot10^{7}$	$7.21\cdot10^{7}$

From experimental and empirical data listed above, indentation modulus E_{IT} has been calculated, from relation (1). Values are shown in Table VI.

Table VI: Data of Young's modulus and indentation modulus of tested metals.

	E /GPa (ref.)	E_{IT} /GPa (HV3)	E_{IT} /GPa (HV30)	E_{IT} /GPa (HV100)
Stainless steel	201.7	153.2	113.9	97.8
Copper alloy	122.6	90.4	69.6	52.9
Aluminum alloy	71.6	68.6	66.1	59.8
Brass	78.9	85.3	74.7	65.4

In the following graphs of Figure 7 the average diagonal and the square root of the contact area, as a function of load, are shown, for all samples.

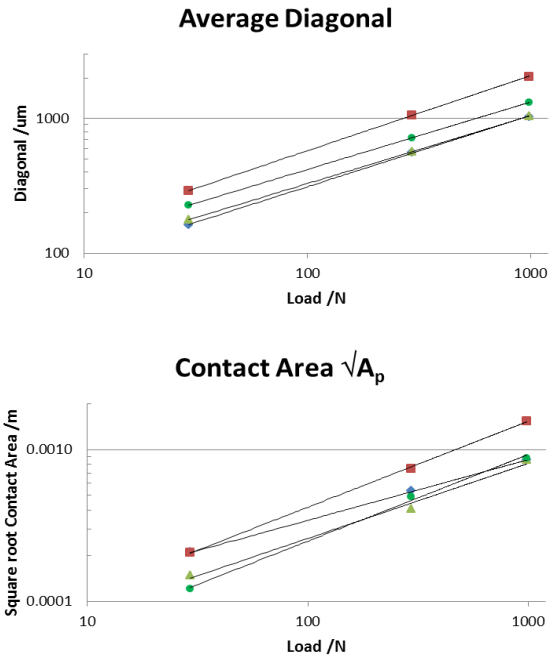

Figure 7: Average diagonal and square root of contact area experimentally determined.

In the following graph of Figure 8, a comparison between the maximum indentation depth h_{MAX} measured by interferometry and the indentation depth h_v measured from the actual Vickers hardness impression, from relation (10).

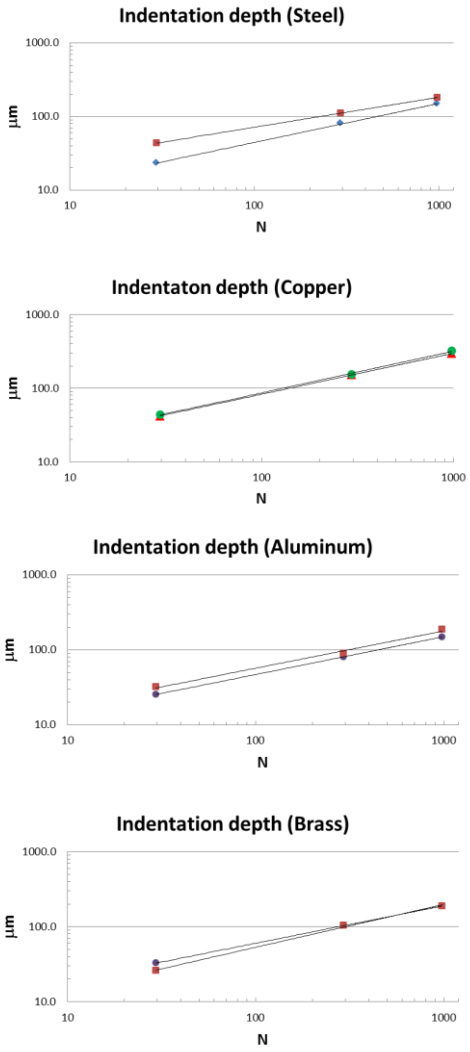

Figure 8: Indentation depth measured by interferometry and by actual impression on the samples.

As it is possible to notice, all experimental data, summarized in Table II-V, show a systematic dependence, as a function of applied load. First evidences suggest that values measured with 3 kg of mass (29.4 N) are less accurate than other values. Nevertheless it is known that, in general terms, the poorly defined tip shape of Vickers indenters at low indentation depths is a cause of hardness measurement errors [18]. More in depth analysis are currently under investigation, involving the validity of the assumption of a load independent value for C_f and further checking the homogeneity of the tested materials.

In the following graph of Figure 9, indentation modulus E_{IT} of each sample, is compared with Young's modulus E. Values of indentation modulus are determined from data listed above, on the basis of relation (1), and data of Young's modulus are evaluated on the basis of relation (11) and (12), from accurate measurements of speed of sound in solids. The observed load-dependence of all experimental data, allows to achieve a load-dependent indentation modulus.

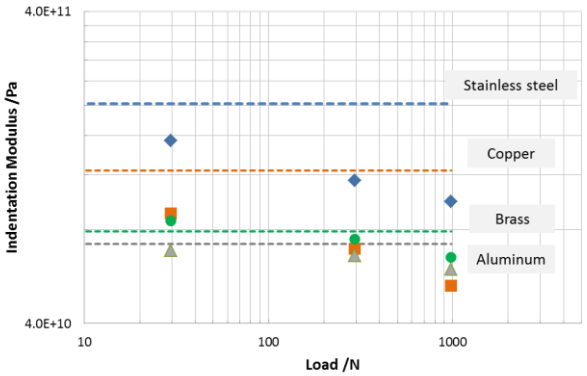

Figure 9: Indentation modulus as a function of load (marker) and dynamic Young's modulus (dotted line).

7. CONCLUSIONS

In this paper it is described a method for the measurement of indentation modulus by using the primary hardness standard machine at INRIM, in the macro-scale range. Indentation modulus is calculated on the basis of Doerner-Nix linear model and from accurate measurements of indentation load, displacement, contact stiffness and Vickers hardness impression imaging. In particular a detailed analysis of frame compliance is performed and commented. Preliminary tests are performed on metallic samples and experimental data and results are carefully reported.

7. ACKNOWLEDGEMENTS

The research leading to these results is conducted in the frame of EMPIR 14IND03 "Strength-ABLE". The EMPIR is jointly funded by the EMPIR participating countries within EURAMET and the European Union.

8. REFERENCES

[1] ISO 14577-11:2002. Metallic materials – Instrumented indentation test for hardness and materials parameters – Part 1: test method.

[2] N.A. Stilwell, D. Tabor, "Elastic recovery of conical indentations," in Proc. of the Physical Society, vol. 78, no. 2, pp. 169-179, 1961.

[3] J.B. Pethicai, R. Hutchings, W.C. Oliver, "Hardness measurement at penetration depths as small as 20 nm," Philosophical magazine, vol. 48, no. 4, pp. 593-606, 1983.

[4] M.F. Doerner, W.D. Nix, "A method for interpreting the data depth-sensing indentation instruments," J. Mater. Res, vol. 1, no. 4, pp. 601-609, 1986.

[5] W.C. Oliver, G.M. Pharr, "An improved technique for determining hardness and elastic modulus using load and displacement sensing indentation experiments," Journal of materials research, vol. 7, no. 06, pp. 1564-1583, 1992.

[6] Y.W. Bao, W. Wang, Y.C. Zhou, “Investigation of the relationship between elastic modulus and hardness based on depth-sensing indentation measurements,” Acta Materialia, vol. 52, pp. 5397–5404, 2004.
[7] J.E. Zorzi, C.A. Perottoni, “Estimating Young’s modulus and Poisson’s ratio by instrumented indentation test,” Materials Science & Engineering A, vol. 574, pp. 25-30, 2013.
[8] J. Prou, K. Kishimoto, A. Constantinescu, “Identification of Young’s Modulus from Indentation Testing and Inverse Analysis,” Journal of Solid Mechanics and Materials Engineering, vol. 4, no. 6, pp. 781-795, 2010.
[9] T. Chudoba, N.M. Jennett, “Higher accuracy analysis of instrumented indentation data obtained with pointed indenters,” Journal of Physics D: Applied Physics, vol. 41, no. 21, 215407, 2008.
[10] C. Ullner, E. Reimann, H. Kohlhoff, A. Subaric-Leitis, “Effect and measurement of the machine compliance in the macro range of instrumented indentation test,” Measurement, vol. 43, no. 2, pp. 216-222, 2010.
[11] R. Cagliero, G. Barbato, G. Maizza, G. Genta, “Measurement of elastic modulus by instrumented indentation in the macro-range: Uncertainty evaluation,” International Journal of Mechanical Sciences, Vol. 101, pp. 161-169, 2015.
[12] K. Herrmann, N.M. Jennett, W. Wegener, J. Meneve, K. Hasche, R. Seemann, “Progress in determination of the area function of indenters used for nanoindentation,” Thin Solid Films, Vol. 377-378, pp. 394-400, 2000.
[13] F. Petit, V. Vandeneede, F. Cambier, “Relevance of instrumented micro-indentation for the assessment of hardness and Young’s modulus of brittle materials,” Materials Science and Engineering A, vol. 456, pp. 252-260, 2007.
[14] G. Barbato, S. Desogus, R. Levi, “Design and performance of a dead-weight standard Rockwell hardness testing machine,” Journal of testing and Evaluation, vol. 6, pp. 276-279, 1978.
[15] A. Germak, C. Origlia, “Metrological characterization of the Vickers Hardness Calibration Machine and Gal-Vision measuring system realised By LTF for NIM (China),” INRIM Tech. Report, no. 16, 2006.
[16] A. Germak, A. Liguori, C. Origlia, “Experience in the metrological characterization of primary hardness standard machines,” in Proc. of HARDMEKO, 2007.
[17] S. Lago, S. Brignolo, R. Cuccaro, C. Musacchio, P.G. Albo, P. Tarizzo, “Application of acoustic methods for a non-destructive evaluation of the elastic properties of several typologies of materials,” Applied Acoustics, vol. 75, pp. 10-16, 2014.
[18] I. Spary, A. Bushby, N.M. Jennett., “On the indentation size effect in spherical indentation,” Philosophical Magazine, vol. 86, no. 33-35, pp. 5581-5593, 2006.